Evaluation of Algebraic Turbulence Models for PNS Predictions of Supersonic Flow Past a Sphere-Cone

Siamack A. Shirazi* and C. Randall Truman†
University of New Mexico, Albuquerque, New Mexico

The Cebeci-Smith and Baldwin-Lomax turbulence models were evaluated for supersonic and hypersonic flow past sphere-cones. Parabolized Navier-Stokes (PNS) predictions were compared with measurements for adiabatic flow at Mach 3 and for cold-wall flow at Mach 5 and 8. Convergence of the numerical simulations to within 1% was ensured by carefully refining the grid spacings and using minimal smoothing. The normal grid spacing near the wall was required to be much smaller than usually accepted values and many grid points were needed in the boundary layer to minimize the effects of even small smoothing. Both turbulence models required careful definition of the boundary-layer thickness in computing the outer eddy viscosity to obtain accurate predictions of surface shear stress and heat transfer. These algebraic models, which produce similar results for subsonic and transonic flows, showed significant differences in these supersonic and hypersonic flows. The sources of these differences were determined to be the forms of near-wall damping, the outer eddy-viscosity formulations, and the effects of outer-layer intermittency.

Nomenclature

$\tilde{a}_\infty$ = freestream speed of sound
$D,\bar{D}$ = van Driest damping, Eqs. (4) and (10)
F = dimensionless "vorticity function" in Baldwin-Lomax model, Eq. (13)
H = dimensionless total enthalpy, $\tilde{H}/\tilde{V}_\infty^2$
K = dimensionless thermal conductivity, $\tilde{K}/\tilde{K}_\infty$, Eq. (2)
K_e = dimensionless effective conductivity, $\tilde{K}_e/\tilde{K}_\infty$, Eq. (2)
$\tilde{L}$ = characteristic or reference length
M_∞ = freestream Mach number, $\tilde{V}_\infty/\tilde{a}_\infty$
N = dimensionless normal distance from the surface, $\tilde{N}/\tilde{L}$
N^+ = dimensionless wall coordinate, $Re_\infty^{1/2}\rho_w(\tau_w/\rho_w)^{1/2}N/\mu_w$
p = dimensionless pressure, $\tilde{p}/\tilde{\rho}_\infty\tilde{V}_\infty^2$
Pr = Prandtl number
Re_∞ = freestream Reynolds number, $\tilde{\rho}_\infty\tilde{V}_\infty\tilde{L}/\tilde{\mu}_\infty$
R_n = nose radius of sphere
St_∞ = Stanton number based on freestream conditions, Eq. (17)
T = dimensionless temperature, $\tilde{T}/\tilde{T}_\infty$
u,v,w = dimensionless velocity components in the Cartesian coordinates, $\tilde{u}/\tilde{V}_\infty$, $\tilde{v}/\tilde{V}_\infty$, $\tilde{w}/\tilde{V}_\infty$
V = dimensionless total velocity, $(u^2+v^2+w^2)^{1/2}$
V_T = dimensionless component of total velocity tangential to surface (including crossflow), $\tilde{V}_T/\tilde{V}_\infty$
x,y,z = dimensionless physical Cartesian coordinates, $\tilde{x}/\tilde{L}$, $\tilde{y}/\tilde{L}$, $\tilde{z}/\tilde{L}$
α = angle of attack
$\gamma,\bar{\gamma}$ = Klebanoff intermittency factor, Eqs. (7) and (14)
δ = dimensionless boundary-layer thickness, $\tilde{\delta}/\tilde{L}$
δ^* = dimensionless kinematic, or "incompressible," displacement thickness, Eq. (6)
θ_c = cone half-angle
κ = von Kármán constant, Eq. (3)
μ = dimensionless coefficient of viscosity, $\tilde{\mu}/\tilde{\mu}_\infty$, Eq. (1)
μ_e = dimensionless effective viscosity, $\tilde{\mu}_e/\tilde{\mu}_\infty$, Eq. (1)
ξ,η,ζ = dimensionless computational coordinates in the streamwise (axial), radial (normal), and circumferential directions
ρ = dimensionless density, $\tilde{\rho}/\tilde{\rho}_\infty$
τ_w = dimensionless wall shear stress, $\tilde{\tau}_w/(\tilde{\mu}_\infty\tilde{V}_\infty/\tilde{L})$
ϕ = meridian angle, = 0 deg windward, 180 deg leeward
$|\omega|$ = dimensionless magnitude of vorticity vector, $|\tilde{\omega}|/(\tilde{V}_\infty/\tilde{L})$

Subscripts and Superscripts

∞ = freestream value
e = edge of boundary layer
i = inner region of boundary layer
max = location of maximum in $F(N)$
o = outer region of boundary layer
t = turbulent
w = wall value
$(\tilde{\ })$ = dimensional quantity

Presented as Paper 87-0544 at the AIAA 25th Aerospace Sciences Meeting, Reno, NV, Jan. 12-15, 1987; received Aug. 14, 1987; revision received March 21, 1988.

*Graduate Research Assistant, Department of Mechanical Engineering. Student Member AIAA.

†Associate Professor, Department of Mechanical Engineering. Senior Member AIAA.

Introduction

In recent years, the development of efficient numerical algorithms has made possible the computation of complex turbulent flowfields about aerodynamic bodies. The parabolized Navier-Stokes (PNS) method[1] used herein is an example of such numerical algorithms for high-speed flows. Turbulence models employed for compressible flows have been based on those developed for incompressible flows. Models used to predict supersonic and hypersonic flows include algebraic, one-equation,[2] and two-equation models.[3-5] Algebraic turbulence models are attractive since the required storage space and computational time are significantly less than these using more sophisticated turbulence models. Moreover, no significant improvement may result from using a two-equation model for attached flows.[3-5]

Two algebraic models were evaluated in the present study. The model developed by Cebeci and Smith[6] has been extended to compressible and three-dimensional boundary layers.[7] This model has been used in boundary-layer,[8,9] viscous shock-layer,[10] and Navier-Stokes[4,5,11] predictions. The difficulty in

defining the edge of the boundary layer led to the development of an algebraic model by Baldwin and Lomax,[12] which was patterned after that of Cebeci and Smith. This model has been widely used for the calculation of turbulent flow in PNS[3,13-17] and Navier-Stokes[4,5,18,19] algorithms. Other mixing length models have been used in boundary-layer[3,8] and PNS[2] predictions, but were not included in this study.

The impetus of the present work was the need to predict turbulent flow at supersonic and hypersonic speeds past slender bodies at angle of attack. A number of predictions of flows past sharp bodies, such as cone and ogive shapes, have been made. The majority of these boundary-layer,[8,13] PNS,[3,13-16,20] and Navier-Stokes[5,19,21] analyses used the Baldwin-Lomax turbulence model. Relatively few predictions of heat transfer for flow past spherically blunted bodies are available. The boundary-layer predictions of Widhopf and Hall[9] at $M_\infty = 5$ for a sphere-cone employed the Cebeci-Smith model, as did the viscous shock-layer prediction by Szema and Lewis[10] for sphere-cones at $M_\infty = 4$–20. Helliwell et al.[2] used the two-layer mixing length in a PNS code to compute flow past a bicone at $M_\infty = 8$. McWherter et al.[17] employed a PNS model with the Baldwin-Lomax turbulence model to compute pressure distributions, forces, and moments for sphere-cones from $M_\infty = 6$–14.

The present work is a numerical study of turbulent flow over sphere-cones at Mach 3-8, as listed in Table 1. This body geometry was chosen since direct comparisons between the turbulent predictions and measurements could be made. Because turbulence models ultimately rely on empirical information, their performance must be evaluated by comparing accurate numerical solutions to high-quality data bases. The quality of the present predictions was ensured through grid refinements in the marching, circumferential, and normal directions, with the effect of smoothing carefully minimized. The data used for comparison herein includes laser-Doppler velocimeter (LDV) measurements[22] of velocity profiles, Preston-probe data for wall shear stress[22] and surface heat-transfer[9,23] data. Predictions of wall shear stress and heat transfer are believed to be good indicators of the performance of the turbulence model.

Numerical Solution

Since the PNS equations are parabolized in the streamwise direction, an efficient marching solution method can be used. The generalized-coordinate PNS code used in this study is a version developed by Tannehill et al.,[1] which is similar to the AFWAL PNS code[24]; the main differences are due to the inclusion of the circumferential viscous terms, the treatment of the pressure term in the subsonic region, and the arbitrary orientation of the (η,ζ) plane in the Tannehill version. The PNS algorithm is first-order accurate in the marching direction ξ and second-order accurate in the η and ζ coordinates. An explicit shock-fitting procedure was used to obtain the outer boundary (bow shock) in each marching step. Boundary conditions at the boundary surface were applied in an approximate implicit fashion and used first-order-accurate approximations to normal derivatives. The original code[1] used second-order-accurate differences to update these boundary conditions before taking the next marching step; however, the marching step size was restricted to be extremely small as the normal grid spacing was reduced. A significant imprvement in stability with respect to marching step size was achieved by using first-order-accurate differences in the "update" procedure to be consistent with those used in the original approximate-implicit boundary conditions.[25]

The Vigneron approximation to the streamwise pressure gradient in the subsonic region of the turbulent boundary layer was employed to permit stable marching of the PNS algorithm.[13] Even though this approach retains only as much of the streamwise pressure gradient as an eigenvalue stability analysis permits, it sometimes caused solutions to be unstable in the initial marching steps. The Tannehill code[1] takes the pressure gradient to be zero in the first few marching steps to overcome this instability. For the results herein, the pressure gradient was neglected for up to 10 marching steps (as denoted in Table 2) to enhance the stability in the development of the flow from the starting solution to the PNS marching solution. Although large oscillations still occurred in the first few marching steps, the effect on the solution far downstream of the start is much less than 1%. The exception is case 2, where the pressure gradient was neglected in only three steps. Since the body length is only about six times the nose radius, the influence of neglecting the pressure gradient in the first few marching steps was as large as 1% at the end of the body.

Table 1 Freestream conditions and sphere-cone geometry for the experimental data considered

Case	Ref.	θ_c, deg	R_n, in.	M_∞	α, deg	$Re_\infty/\tilde{L}$, per ft	$\tilde{T}_\infty$, °R	$\tilde{P}_\infty$, lb/in.^{2}	$\tilde{T}_w$, °R
1a	22	7	0.65	3	0	2.14×10^{6}[a]	203	0.40	(Adiabatic)
1b	22	7	0.65	3	4	2.14×10^{6}[a]	203	0.40	(Adiabatic)
2	9	9	2.5	5	0	18.3×10^{6}	133	1.07	185
3a	23	7	0.5	8	0	3.7×10^{6}	98	0.083[a]	540
3b	23	7	0.5	8	10	3.7×10^{6}	98	0.083[a]	540

[a]Calculated from other freestream conditions given in table.

The algebraic turbulence models that were implemented in the implicit, noniterative algorithm employed two upstream planes to compute the metrics and Jacobians of the transformation. Thus, the PNS algorithm requires two initial-solution planes for which the inviscid region of the flowfield is supersonic. The starting-solution planes for the present study were provided by a blunt-body (thin-layer Navier-Stokes)[26] solution for flow over a sphere. A preprocessor program[17] was used to rotate the blunt-body solution to the correct angle of attack for the sphere-cone, to match the spherical nose and conical afterbody, and to interpolate to obtain the two initial planes. Turbulent flow calculations were started from the sphere-cone tangency point using these planes.

Explicit fourth-order and implicit second-order smoothing terms are used in the Tannehill PNS code to damp oscillations associated with the numerical algorithm.[1] Small values of the explicit smoothing parameter were used when necessary; no implicit smoothing was necessary. Values of the smoothing parameters for each case are listed in Table 2. The explicit smoothing was chosen as the minimum value that removed oscillations evident in the distributions of pressure and cross-flow velocity in the normal direction. Solutions that used smaller values eventually developed streamwise oscillations in wall shear stress and heat transfer. The effects of larger explicit smoothing were also studied using values from four to eight times larger. These solutions differed by less than 1% if the normal grid spacing was sufficiently small; in general, this required 89 grid points. The explicit smoothing should damp any oscillations that might appear in regions where viscous damping is small. With coarse grid spacing, however, the smoothing had a significant effect on the predictions of wall shear stress and heat transfer. Clearly, the truncation error in the smoothing term must be minimized as well.

For the present numerical results, the computational planes were chosen to be normal to the body axis ξ. The η (radial) lines were generated using straight-line rays emanating from the body that were uniformly distributed in the ζ (circumferential) direction from $\phi = 0$ deg (windward) to $\phi = 180$ deg (leeward). Radial grid points were clustered near the wall according to a stretching parameter β.[1] The clustering was applied to the radial grid spacing normalized by the local shock-standoff distance and held fixed in the circumferential direction and through the marching steps. Thus, the normal grid spacing increased as shock-standoff distance increased in the marching direction. The step size in the marching direction was taken to have geometric growth according to $\Delta\xi_n = k\Delta\xi_{n-1}$. Nonuniform spacing was used for cases that required a small marching step size near the start. Values of all parameters describing the grid spacings are listed in Table 2.

Table 2 Input parameters for PNS predictions

Case	Initial ξ, in.	Final ξ, in.	ξ steps	$\Delta\xi_1$, in.	k[a]	η grid points	β	ζ grid points	ϵ_E[b]	ξ steps with $dp/d\xi = 0$
1a	0.573	15.555	2000	7.49×10^{-3}	1	89	1.001	5	0.0045	10
1b	0.573	15.555	2000	2.07×10^{-3}	1.0011	89	1.001	47	0.0045	10
2	2.109	13.434	500	2.26×10^{-3}	1	89	1.00005	5	0.0069	3
3a	0.439	35.0	2000	1.29×10^{-3}	1.002	89	1.001	5	0.0035	10
3b	0.439	35.0	2000	1.29×10^{-3}	1.002	89	1.002	47	0.0035	10

Note: ξ = streamwise along body axis, η = normal to body axis, ζ = circumferential.
[a]$\Delta\xi_n = k\Delta\xi_{n-1}$. [b]$\epsilon_E$ = explicit smoothing parameter[1]; no implicit smoothing.

The accuracy of the numerical solutions was carefully demonstrated for each case with each turbulence model by independently refining the grid in the marching, circumferential, and normal directions. The procedure used to determine the rate of convergence is described by Keller[27] and Blottner.[28] Successive grid refinement coupled with Richardson extrapolation was used to perform an "extrapolation to zero meshwidth."[27] The truncation error in each prediction was computed by comparing it to the "exact" (extrapolated) value. The quantities examined included wall pressure and either shear stress or heat transfer at the surface.

Figure 1 shows the results for refining the normal grid spacing for case 2 (described below). The predictions used to compute the error all used the same marching and circumferential grid spacings, smoothing, and normal grid stretching parameter β. Each prediction was compared to a value formed by extrapolating from the 89- and 177-grid-point solutions to the "exact" ($\Delta\eta\to0$) solution.[27] The predictions employing each turbulence model demonstrate second-order accuracy with respect to the normal grid spacing, although coarse-grid solutions deviate from the theoretical behavior. The fact that the error in the predictions using one turbulence model was larger than the error using the other model is not significant since the order was reversed for other cases. Values of N^+ nearest the wall for each grid spacing are shown on Fig. 1. This case requires approximately 89 grid points distributed such that N^+ near the wall is one or less to reduce the truncation error due to normal grid spacing to about 1%. Smaller grid spacings were required for other cases, as discussed below.

These convergence studies were successful only when very fine normal grid spacing was used as the marching grid spacing was varied. Moreover, the normal gradients of velocity and temperature needed to obtain wall shear stress and heat transfer were in significant error at the coarse-grid spacings if computed using the transformed coordinates. It was discovered that the truncation error in the velocity or temperature values from which the gradients were computed was compounded by truncation error in certain terms in the metrics and Jacobians of the transformation. The convergence studies therefore were made with normal gradients computed using physical coordinates. It was also demonstrated that as the normal grid spacing was refined, the difference between the normal gradients computed by these two methods vanished.

The results presented herein used grid spacings for which the truncation error with respect to grid spacing in each direction was estimated to be less than 1%. These stringent accuracy requirements are necessary for a careful evaluation of turbulence models in which the cumulative errors due to normal, streamwise, and circumferential grid spacings as well as smoothing must be minimized. Moreover, streamwise grid spacings that were much smaller than required by grid refinement studies were employed to reduce oscillations near the start and allow the use of smaller smoothing parameters.

Turbulence Models

The dimensionless effective viscosity and thermal conductivity are defined as

$$\mu_e = \mu_t + \mu \tag{1}$$

and

$$K_e = [(\mu_t Pr)/Pr_t] + K \tag{2}$$

where μ_t is the dimensionless turbulent viscosity and the dynamic viscosity μ is obtained from Sutherland's law.[6] The turbulent Prandtl number Pr_t was assumed[6] to be 0.9. The turbulent viscosity coefficient μ_t was obtained using the two-layer eddy-viscosity models of Cebeci and Smith[6] (CS) and Baldwin and Lomax[12] (BL). These two algebraic models are quite similar; they differ primarily in the choice of length and velocity scales in the outer layer. The outer formulation of the BL model is based upon the distribution of vorticity rather than velocity as in the CS model.

Cebeci-Smith Turbulence Model

The algebraic model extended to three-dimensional and compressible flows by Cebeci et al.[7] was used in this study. The CS inner formulation is given by the Prandtl-van Driest relation

$$(\mu_t)_i = Re_\infty \rho (\kappa N D)^2 \left| \frac{\partial V_T}{\partial N} \right| \tag{3}$$

where N is the local distance measured normal to the body surface and $\kappa = 0.4$ is the von Kármán constant. The tangential component of dimensionless total velocity V_T includes a cross-flow contribution. In the van Driest damping

$$D = 1 - \exp\left[\frac{-N^+ (\rho/\rho_w)^{1/2} (\mu_w/\mu)}{26} \right] \tag{4}$$

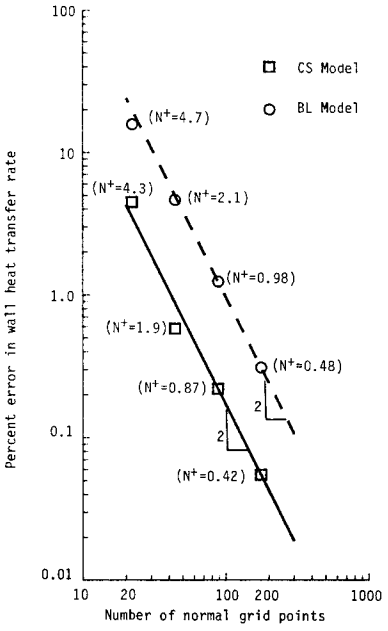

Fig. 1 Percent error in wall heat transfer rate vs number of normal grid points at $M_\infty = 5$, $\alpha = 0$ deg, $\tilde{x} = 13.4$ in. (case 2). (N^+ denotes value nearest the wall.)

the factor $(\rho/\rho_w)^{1/2}(\mu_w/\mu)$ accounts for compressibility in the inner region of the viscous layer. Similar forms of D have been used in several studies of supersonic and hypersonic flows.[8-11,29] This factor can be approximated by $(T_w/T)^2$, by using the Sutherland expression for viscosity and the ideal-gas relation. This form illustrates the effect of changes in temperature near the wall upon the damping. When the temperature exceeds the wall temperature, the van Driest damping extends to larger values of N^+. Conversely, for a fixed value of N^+ the damping D will be smaller for $T > T_w$. The effect upon the predictions can be significant depending on the temperature distribution near the wall.

The outer layer in the CS model is described by the Clauser-Klebanoff formulation

$$(\mu_T)_o = Re_\infty(0.0168)\rho(V_T)_e\delta^*\gamma \tag{5}$$

where $(V_T)_e$ is evaluated at the edge of the boundary layer δ. The determination of the boundary-layer edge is discussed in a later section. The kinematic or "incompressible" displacement thickness δ^* was obtained from the expression[6] for axisymmetric flow past a body of radius r_b

$$\delta^* = -r_b + \left[(\delta + r_b)^2 - 2\int_{r_b}^{\delta + r_b}(u/u_e)r\,dr\right]^{1/2} \tag{6a}$$

where

$$r = (y^2 + z^2)^{1/2} \tag{6b}$$

and u_e is the velocity in the x direction evaluated at δ. This displacement thickness is measured in a direction normal to the body axis; the small correction to yield a distance normal to the body surface was neglected. The Klebanoff intermittency factor

$$\gamma = \left[\frac{1}{1 + 5.5(N/\delta)^6}\right] \tag{7}$$

models the decrease in eddy viscosity near the edge of the boundary layer. The turbulent viscosity coefficient in Eqs. (1) and (2) was obtained by

$$\mu_t = \begin{cases}(\mu_t)_i & N \le N_c \\ (\mu t(\mu_t)_o & N > N_c\end{cases} \tag{8}$$

where N_c is the smallest value of N where $(\mu_t)_i = (\mu_t)_o$.

Baldwin-Lomax Turbulence Model

The other algebraic turbulence model used in this study is due to Baldwin and Lomax[12] (BL). The inner formulation, which is similar to Eq. (3), is

$$(\mu_t)_i = Re_\infty\rho(\kappa N\bar{D})^2|\omega| \tag{9}$$

where $|\omega|$ is the magnitude of the local vorticity vector. The magnitude of the vorticity is very similar to the normal gradient of the tangential velocity used in the CS model; they are identical under a thin-shear-layer assumption. The van Driest damping in Eq. (9) is

$$\bar{D} = 1 - \exp(-N^+/26) \tag{10}$$

The van Driest damping in Eqs. (4) and (10) is identical for isothermal, incompressible flow.

The outer formulation of the BL model replaces the Clauser formulation used in the CS model by

$$(\mu_t)_o = Re_\infty(0.0168)\rho C_{cp}F_{\text{wake}}\bar{\gamma} \tag{11}$$

where $C_{cp} = 1.6$ is an additional constant introduced by Baldwin and Lomax.[12] For attached shear flows,

$$F_{\text{wake}} = N_{\max}F_{\max} \tag{12}$$

The quantities $N_{\max}$ and $F_{\max}$ correspond to the values at the location of the maximum value in the "vorticity function"

$$F(N) = N|\omega|\bar{D} \tag{13}$$

within the boundary-layer region, where $\bar{D}$ is given by Eq. (10). Quadratic interpolation was used to determine $F_{\max}$ and $N_{\max}$ from the discrete $F(N)$ and N distributions. It was found to be necessary to limit the search for $F_{\max}$ to the boundary-layer region. This criterion for choosing the maximum value of $F(N)$ will be discussed in more detail with the results. The Klebanoff intermittency factor is given by

$$\bar{\gamma} = \left[\frac{1}{1 + 5.5(C_{\text{Kleb}}N/N_{\max})^6}\right] \tag{14}$$

where $C_{\text{Kleb}} = 0.3$. The constants C_{cp} and C_{Kleb} were determined by the calibration for transonic flat plates described by Baldwin and Lomax.[12] The ratio $N_{\max}/C_{\text{Kleb}}$ replaces δ used in the Klebanoff intermittency factor given by Eq. (7). This quantity represents a boundary-layer thickness, nonetheless, and must be carefully studied. Thus, the boundary-layer thickness must be determined to evaluate $N_{\max}$, $F_{\max}$, and $\bar{\gamma}$ in the BL model, as will be discussed below. The turbulent viscosity coefficient is defined in the same manner as Eq. (8).

One of the problems that has arisen in the implementations of the Baldwin-Lomax model is some ambiguity in determining the peak in the distribution of the vorticity function $F(N)$.[15,16] This is discussed in the Results section. In addition, some of the constants appearing in the Baldwin-Lomax outer formulation have been reported to depend on the flow Mach number.[18]

Determination of δ

As discussed above, accurate determination of the boundary-layer thickness is required to implement both the CS and BL models. When the velocity in the inviscid part of the shock-layer region of a supersonic flow is not constant, it is difficult to define the boundary-layer edge in the usual way. However, the total enthalpy should be constant within the inviscid part of the shock layer region. For cold-wall cases where a large total enthalpy gradient was observed within the boundary-layer region, the definition of the boundary-layer edge based upon the total enthalpy[10] was

$$\delta = \min N, \text{ where } \begin{cases}\dfrac{|H - H_\infty|}{|H_\infty - H_w|} = 0.005 & \text{(15a)} \\ \dfrac{du}{d\eta} = 0 & \text{(15b)}\end{cases}$$

The total enthalpy should increase from its wall value H_w to a constant value in the inviscid region H_∞. Truncation error may cause the total-enthalpy profile to have a local maximum in the region where the edge of the boundary layer is being sought. Studies showed that this local maximum in H vanished as the normal grid was refined. Thus, the search for δ using Eq. (15a) was limited to the region below this peak. Equation (15b) was used to avoid the possibility of computing a negative δ^* when u has a local maximum inside the boundary layer. The boundary-layer edge was determined by quadratic interpolation within the discrete total-enthalpy or velocity distribution.

For adiabatic and hot-wall cases where total enthalpy changes are small within the boundary layer, determination of the boundary-layer edge becomes more difficult and somewhat arbitrary. A literature survey that revealed several ways to

define the boundary-layer edge was discussed by Shirazi and Truman.[30] These criteria include choosing the boundary-layer edge where 1) the change in velocity is small,[11] 2) the vorticity is a small fraction of its wall value,[21] and 3) the product of shear stress and vorticity is small.[10] Since each criterion is necessarily arbitrary, none appeared to be universal. Thus, in the present work, the boundary-layer thickness for adiabatic wall conditions was chosen as the value of N where the local velocity is 0.95 times the maximum velocity within the shock-layer region u_M, i.e.,

$$\delta = N \text{ where } u/u_M = 0.95 \tag{16}$$

While the factor 0.95 is arbitrary, this criterion is in good agreement with experimental values from Ausherman et al.[22] (case 1) at zero angle of attack and from the windward to yaw planes at $\alpha = 4$ deg. This criterion does not, however, give suitable values for δ for cases 2 and 3, which are not adiabatic. The factor 0.95 is not expected to be universal, even for adiabatic flows.

Data Used for Comparison

Case 1: Adiabatic Wall, $M_\infty = 3$

Ausherman et al.[22] made turbulent flow measurements for a spherically blunted cone at several angles of attack in an adiabatic Mach 3 flow. Laser-Doppler velocimeter (LDV) measurements of turbulent velocity profiles, turbulent intensities, and Reynolds stresses were made at a single axial station for freestream Mach numbers of 3 and 5, meridian angles of 0–135 deg, and angles of attack of 0 deg (case 1a) to 4 deg (case 1b). Wall-shear-stress and surface-pressure distributions vs roll angle were measured at five axial stations by a Preston probe and static pressure orifice, respectively. The boundary layer was tripped near the blunt nose to ensure a fully turbulent boundary layer at the model measurement stations. Near-equilibrium wall temperatures were also measured.

Case 2: Cold Wall, $M_\infty = 5$

Widhopf and Hall[9] made transitional and turbulent heat-transfer measurements on a blunt cone with constant wall temperature at Mach 5. The flow underwent transition to turbulent flow along the sphere without tripping. Data were taken at several freestream Reynolds numbers and angles of attack, but did not extend much over the conical portion of the sphere-cone. Comparisons were made with data at one Reynolds number and zero angle of attack. The uncertainty of the cold-wall heat-transfer measurements made with chromel-alumel thermocouples was estimated to be within $\pm$ 10%.[9]

Case 3: Cold Wall, $M_\infty = 8$

The AEDC Tunnel B data for the HYTAC sphere-cone reported by Carver[23] includes heat transfer for constant wall temperature at Mach 8. Boundary-layer trips near the sphere-cone juncture were used to obtain fully turbulent flows. Cold-wall heat-transfer measurements were obtained with coaxial thermocouple surface-mounted gages for 0 deg (case 3a) to 10 deg (case 3b) angle of attack. The uncertainty in heat-transfer measurements was estimated to be 15%.[23]

Results

Computation time for a typical turbulent-flow prediction was approximately 4×10^{-3} s CPU s/grid point on a CDC Cyber 855. Table 1 shows the freestream conditions and geometry for each case. A perfect-gas model has been used to represent the properties of air. The ratio of specific heats of 1.4 and $Pr = 0.72$ were assumed for all cases. Table 2 lists the input parameters to the PNS code for the results presented herein. The normal grid spacing was chosen so that N^+ nearest the wall was allowed to be as large as 1 near the end of the cone. The exception was case 3 where a smaller grid spacing was required to resolve the temperature peak near the wall. In case 3a, the largest N^+ near the wall was about 0.3, while in case 3b it varied circumferentially between about 0.6 and 0.9. For axisymmetric cases ($\alpha = 0$ deg), five circumferential planes were required to implement the grid distribution. The last column indicates the number of marching steps near the start in which the pressure gradient was taken to be zero, as discussed above in the description of the numerical solution.

Case 1: Adiabatic Wall, $M_\infty = 3$

Measured and predicted tangential velocity profiles for case 1a, in which $\alpha = 0$ deg, are shown in Fig. 2. The computed boundary-layer thicknesses were about 5% of the shock-layer thickness of about 5.6 in. Results from both turbulence models show that the tangential velocity was somewhat underpredicted near the wall and only slightly overpredicted away from the surface. The CS model prediction was marginally better than that using the BL model, although the differences were small. The wall temperature and pressure were predicted to within 1.5% by both models except at the first measurement station. The eddy viscosity in the CS model was larger than that in the BL model in both the inner and other regions and resulted in a larger predicted wall shear stress, as shown in Fig. 3. The CS predictions agreed within 5% with the Preston-tube data, while the BL predictions were about 15% low. The eddy viscosity in the inner region was larger in the CS model by as much as 30% because of the compressible form of the van Driest damping. For this adiabatic flow, the temperature through the boundary layer dropped off sharply from its wall value, which caused the van Driest damping D in the CS model to be larger (i.e., closer to 1) than $\bar{D}$ in the BL model. How-

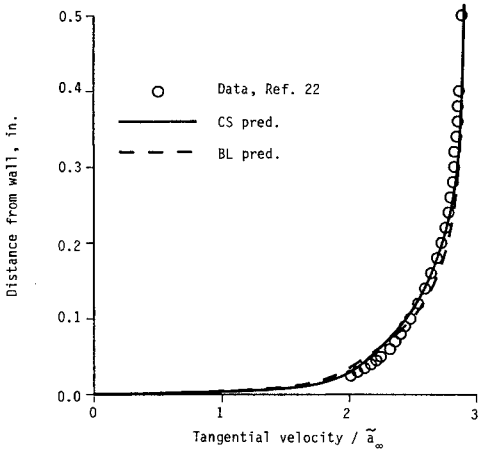

Fig. 2 Tangential velocity vs distance from wall at $M_\infty = 3$, $\alpha = 0$ deg, $\tilde{x} = 15.6$ in. (case 1a).

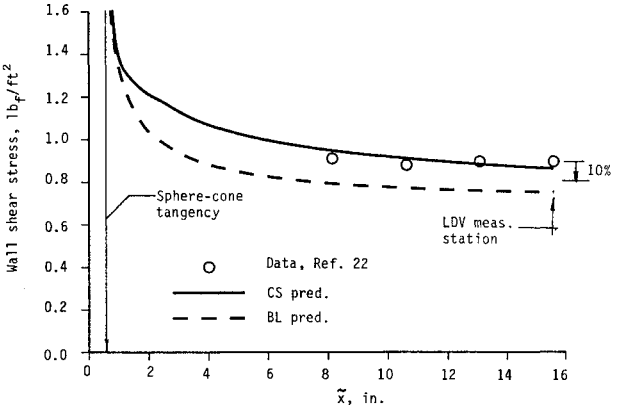

Fig. 3 Wall shear stress vs body axis distance from nose at $M_\infty = 3$, $\alpha = 0$ deg (case 1a).

ever, the difference between the predictions of wall shear stress was primarily due to the eddy viscosity in the outer region, which was larger in the CS model than in the BL model by about 50%. Since δ and $N_{max}/0.3$ were comparable, the effects of intermittency were about the same in each model. Thus, the difference in outer eddy viscosities resulted from the difference in magnitudes of $C_{cp}N_{max}F_{max}$ in the BL model and $\delta^*(V_T)_e$ in the CS model. Neither prediction was sensitive to the intermittency; with $\gamma \equiv 1$, the predicted wall shear stress increased only about 1%. This insensitivity resulted because the maximum outer eddy viscosity was reached before the intermittency began to have significant effect.

The predictions for the sphere-cone at angle of attack were similar to those for $\alpha = 0$ deg, including the relative size of the eddy viscosity in the CS model to that in the BL model. The agreement between predicted and measured streamwise velocity profiles was similar to Fig. 2. Figure 4 shows the circumferential distribution of wall shear stress near the end of the body for case 1b ($\alpha = 4$ deg). The circumferential variation in the data was much larger than that predicted by either turbulence model. The CS and BL models underpredicted the shear stress on the windward side by 14 and 23%, respectively. The shear stress was overpredicted by the CS and BL models on the leeward side by 20 and 2%, respectively. A similar comparison was reported[20] for a secant-ogive-cylinder-boattail body at $M_\infty = 3$ and $\alpha = 4.2$ deg. The Preston-tube measurements of wall shear stress have an uncertainty of at least 10%[31]; since the calibration was made at zero angle of attack,[22] greater uncertainty might be assigned to this data. Reducing the circumferential grid spacing from $\Delta\phi = 4$–2 deg changed the wall shear stress less than 1%. No crossflow separation was predicted.

The crossflow velocity distributions in the BL and CS models were quite similar. At $\phi = 90$ deg, where crossflow was largest, the velocity was overpredicted by as much as 40% near the wall. The magnitude of the crossflow velocity was, however, only about one-tenth that of the streamwise component. The variation of pressure coefficient with meridian angle is shown in Fig. 5. Both turbulence-model predictions were in good agreement with the experimental data. This demonstrates that surface pressure is not, in general, a good indicator of solution accuracy.

Case 2: Cold Wall, $M_\infty = 5$

In this case, heat transfer near the sphere-cone tangency point was significantly overpredicted when F_{max} was obtained by searching throughout the shock layer. A large N_{max} near the shock was selected so that $(\mu_t)_o$ was much too large near the start and in subsequent marching steps. This problem was eliminated by ignoring points outside the boundary layer in the search for the maximum in $F(N)$ along each radial ray. The boundary-layer thickness δ determined by Eq. (15) was used to identify grid points outside the boundary layer since N_{max} was expected to be smaller than δ. This modified BL model was adopted for all the predictions to prevent the solution of unrealistically large N_{max} and the consequent computation of very large $(\mu_t)_o$. The starting solution interpolated from the blunt-body solution also caused a small oscillation in the normal distribution of $F(N)$ through the boundary layer. Several local maxima in $F(N)$ were observed in the PNS starting solution; the largest was used as F_{max} since it was within δ. This oscillation disappeared within the first few marching steps downstream of the starting solution.

Heat-transfer predictions that began at the sphere-cone juncture along with experimental data on the sphere and cone are shown in Fig. 6. The CS predictions fell within the uncertainty of the data and the BL predictions were about 20% large than the CS values. The eddy viscosity in the inner region was about two times larger in the BL model than in the CS model. This large difference resulted from the van Driest damping, because the temperature increased to a value about twice as large as the wall value within the inner region. Downstream of the starting region the maximum eddy viscosity in the outer region of the BL model was only about 10% larger than in the CS model. However, near the start the outer eddy viscosities were also significantly different. The outer eddy viscosity in the BL model at $S/R_n \approx 1.8$, for example, was about half that

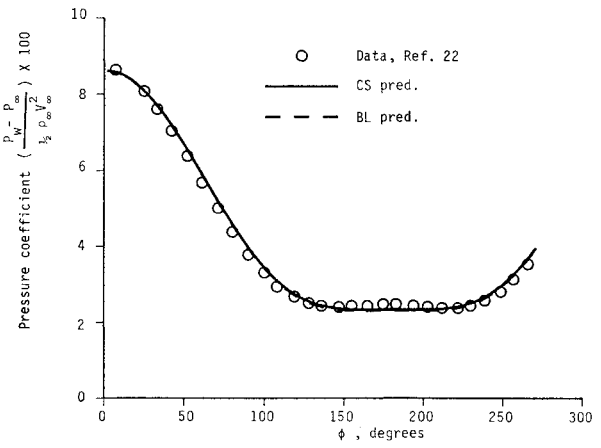

Fig. 5 Pressure coefficient vs roll angle at $M_\infty = 3$, $\alpha = 4$ deg, $\tilde{x} = 15.6$ in. (case 1b).

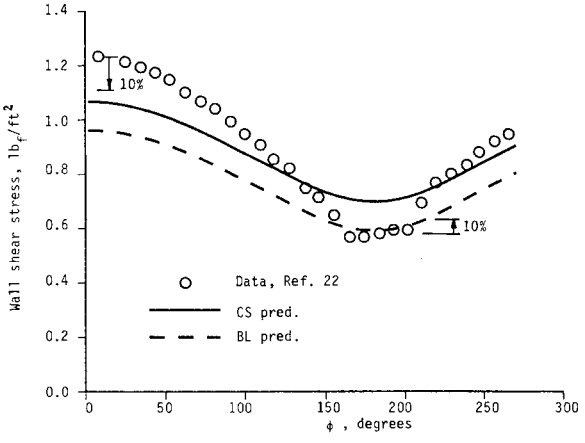

Fig. 4 Wall shear stress vs meridian angle at $M_\infty = 3$, $\alpha = 4$ deg, $\tilde{x} = 15.6$ in. (case 1b).

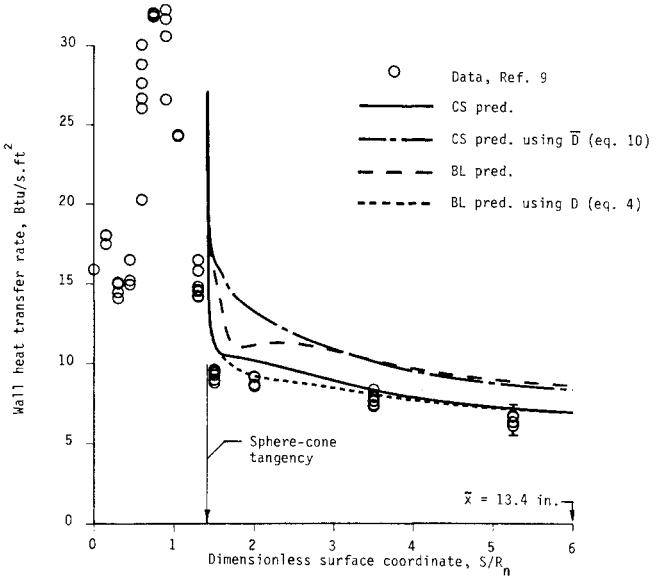

Fig. 6 Wall heat transfer rate vs surface coordinate at $M_\infty = 5$, $\alpha = 0$ deg (case 2a).

in the CS model. Predictions using the BL model with the compressible (CS) form of damping and the CS model with the incompressible (BL) form are also shown in Fig. 6. These predictions confirm that the difference between the two models was almost entirely due to the form of damping used. Although $N_{max}/0.3$ was nearly twice the value of δ, both were relatively large. Thus, the intermittency in the CS model caused the eddy viscosity to drop off at a relatively large value of N. Predictions of heat transfer in the CS and BL models with $\gamma \equiv 1$ and $\tilde{\gamma} \equiv 1$ were only about 2 and 0.2% larger, respectively.

Case 3: Cold Wall, $M_\infty = 8$

Predictions and experimental data for the Stanton number for case 3a ($\alpha = 0$ deg) are shown in Fig. 7. The Stanton number was defined as[23]

$$St_\infty = \frac{\text{heat-transfer rate at the wall}}{\tilde{\rho}_\infty \tilde{V}_\infty [\tilde{h}(\tilde{T}_o) - \tilde{h}(\tilde{T}_w)]} \tag{17}$$

where the enthalpies $\tilde{h}(\tilde{T})$ are air table values. The difference between the BL and CS predictions was similar to that in case 2. However, the difference in predictions for case 3a was due to the intermittency as well as the van Driest damping. The eddy viscosities in the inner region showed the effects to temperature upon the van Driest damping. The temperature distribution had a maximum very near the wall ($N^+ \approx 10$) and the temperature was larger than the wall value throughout the inner layer. Thus, the inner eddy viscosity in the CS model was about 25% smaller than in the BL model. Since $N_{max}/0.3$ was about twice the value of δ, intermittency in the CS model caused the maximum eddy viscosity in the outer region to be about 30% smaller than in the BL model and to decrease rapidly at relatively small N. A CS prediction with no intermittency ($\gamma \equiv 1$) is shown for comparison; there was little change in the BL prediction with $\tilde{\gamma} \equiv 1$. The Stanton number predictions near the end of the body were smaller than the measured values by about 16 and 8% in the CS and BL models, respectively. Since the maximum temperature occurs at $N^+ \approx 10$, the importance of using a small grid spacing near the wall is clear. The error in predicted heat transfer for N^+ near the wall larger than about 1 was large.

Predicted and measured heat transfer for case 3b ($\alpha = 10$ deg) are shown in Figs. 8 and 9. As in case 3a, the agreement between the BL and CS models with $\gamma \equiv 1$ is quite good. The CS model (with intermittency) performed relatively better downstream of the starting region than for $\alpha = 0$ deg (case 3a), because the outer eddy viscosities in the CS and BL models were more nearly equal. Specifically, the value of $N_{max}/0.3$ was only about 50% larger than δ. Figure 8 shows that on the windward side both the CS with $\gamma \equiv 1$ and BL models show good agreement with the experimental data. On the leeward size, however, the Stanton number is underpredicted by about 20% downstream of the sphere-cone tangency plane. The predictions sharply disagree with the experimental data near the sphere-cone tangency plane. This is probably due to the prediction of fully turbulent flow beginning at the tangency plane, while the experimental flow was tripped to turbulence just downstream of that plane.

The agreement between the measured and predicted circumferential variation in heat transfer near the end of the body ($\tilde{x} = 28.5$ in.) was quite good as shown in Fig. 9. The Stanton number was underpredicted on the windward side at this streamwise station by 7, 5, and 3% in the CS, BL, and CS with $\gamma \equiv 1$ models, respectively. The predictions were in good agreement with the data up to the crossflow-separated region ($\phi \gtrsim 150$ deg). Some difficulties arose in determining the outer length scale (δ or N_{max}) in the crossflow-separated region in the CS and BL models, but not with the CS with $\gamma \equiv 1$ model. These difficulties (described below) were not affected by reducing the circumferential grid spacing. Furthermore, the estimated location of the primary crossflow separation varied by no more than 3 deg in predictions with 47, 69, and 93 circumferential grid points in which $\Delta\phi$ varied from 4 down to 2 deg. Secondary and tertiary separation regions were not clearly resolved with these grid spacings, although Degani and Schiff[16] used a circumferential grid spacing of $\Delta\phi = 2.5$ deg to resolve the leeward-side vortex structure on pointed bodies at angle of attack.

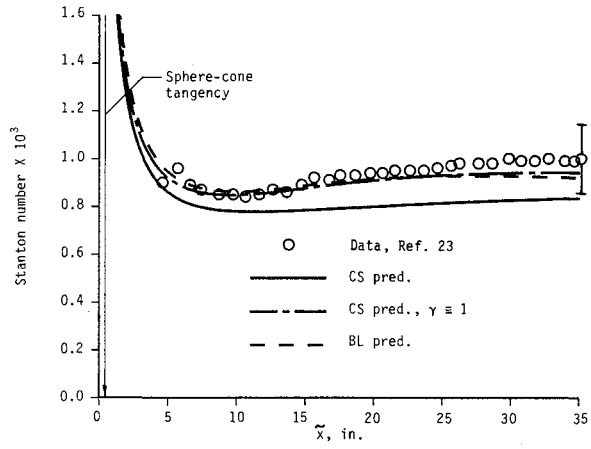

Fig. 7 Stanton number vs body axis distance from nose at $M_\infty = 8$, $\alpha = 0$ deg (case 3a).

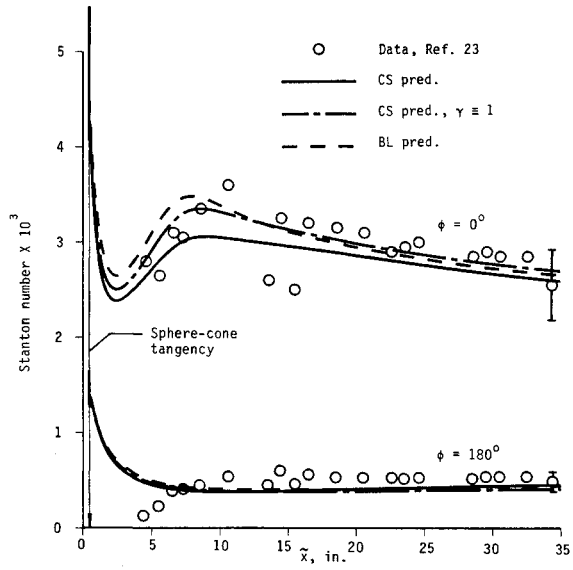

Fig. 8 Stanton number vs body axis distance from nose at $M_\infty = 8$, $\alpha = 10$ deg (case 3b).

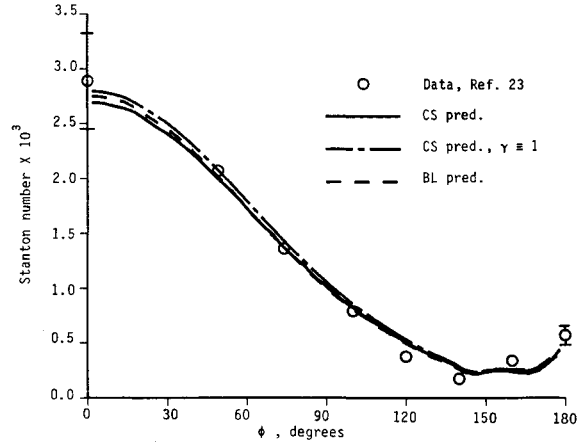

Fig. 9 Stanton number vs meridian angle at $M_\infty = 8$, $\alpha = 10$ deg, $\tilde{x} = 28.5$ in. (case 3b).

Defining δ and N_{max} in the crossflow-separated region was somewhat uncertain in the CS and BL models. In the CS prediction, a peak in streamwise velocity developed at about half the distance computed for δ using the total-enthalpy criterion [Eq. (15a)]; according to Eq. (15b), the peak then determined the boundary-layer thickness with a resulting sharp decrease in outer eddy viscosity. This effect propagated downstream as δ became smaller and several local maxima appeared in the streamwise velocity profile. The circumferential variation of δ (and thus δ^* and μ_t) became somewhat erratic in the crossflow-separated region. This problem did not arise in the CS model with $\gamma \equiv 1$. In the BL model, $F(N)$ became quite large in this region with as many as three peaks within the boundary layer. The criterion which selected F_{max} as the largest value within the boundary layer resulted in N_{max} as large as half the shock-layer thickness so that there was effectively no intermittency. This coupled with the large N_{max} and F_{max} resulted in dimensionless eddy viscosities as large as 4000. Despite the large differences in the eddy-viscosity distributions in the CS and BL models, the predictions of heat transfer in the crossflow-separated region were remarkably similar.

Discussion and Conclusions

Parabolized Navier-Stokes (PNS) predictions of turbulent flow past sphere-cones have been compared with measurements at Mach 3-8. The purpose of this study was to make a careful evaluation of the algebraic Cebeci-Smith (CS) and Baldwin-Lomax (BL) turbulence models for attached flow in the supersonic and hypersonic regimes. While predictions using the two models were generally similar, some important differences arose. These differences were primarily due to the outer-length scale, the inner-layer damping, and the outer-layer intermittency in the Mach 3, 5, and 8 cases, respectively. Ways have been identified in which these algebraic models can be implemented in order to significantly improve predictions of wall shear stress and heat transfer.

The numerical accuracy of the predictions was carefully established to be within 1%. Grid refinement in the normal direction determined that extremely small grid spacings were required, i.e., $N^+ \lesssim 1$ near the wall. Moreover, a relatively large number of grid points was required in the boundary layer to accurately resolve wall shear stress and heat transfer as well as to minimize the effects of smoothing. The predictions used 89 grid points in the shock layer, of which 45-60 were in the boundary layer. Extremely small values of the explicit smoothing parameter were sufficient and no implicit smoothing was needed. Such stringent requirements were appropriate for this evaluation of turbulence models, but are certainly not necessary for engineering predictions. Even so, the grid refinements performed herein may allow an a priori estimate of the truncation error associated with grid spacing for a particular application. For example, in case 3a, using $N^+ \approx 1.2$ near the wall with 45 grid points resulted in errors of about 3%; it is clear that the usually accepted value of $N^+ \approx 4$ near the wall would be much too large.

Care must be taken in selecting the peak in the vorticity function $F(N)$ in the BL model, particularly near the start. Problems in the initial marching steps were observed because the formation of $F(N)$ requires the numerical differentiation of velocities interpolated from the blunt-body starting solution. Moreover, the vorticity function may increase through the shock-layer region. The selection of the peak in $F(N)$ must therefore avoid large values outside the boundary layer. Limiting the search for the maximum in $F(N)$ to the boundary layer, as determined by either Eqs. (15) or (16), was found to resolve these difficulties. The single exception was for case 3b in the region of the crossflow separation. A general criterion for N_{max} and F_{max} in a region of crossflow separation has not yet been achieved, although for some specific cases[15,16] satisfactory results have been obtained. These problems in identifying the maximum in the vorticity function suggest that the boundary-layer thickness must be accurately determined in the Baldwin-Lomax model just as in the Cebeci-Smith model.

The compressibility factor in the CS form of the van Driest damping had a significant influence on the inner eddy viscosity in all cases. This difference between the two models was the dominant factor in the Mach 5 case, where temperature variations in the viscous layer were largest. In the Mach 3 and 5 cases, using the compressibility factor resulted in better agreement with the data. In the Mach 8 case, it tended to have a small, opposite effect on heat transfer, which agrees with the observations of Bushnell et al.[29] for hypersonic flows.

The effect of intermittency was most important for the Mach 8 case in the CS model. Indeed, in other cases the intermittency had little influence because the boundary-layer thickness δ or $N_{max}/0.3$ was large enough that the maximum eddy viscosity was not significantly affected. For the CS model predictions at Mach 8, however, the maximum outer eddy viscosity increased substantially for $\gamma \equiv 1$. An intermittency profile that is uniform across the boundary layer ($\gamma \equiv 1$) can be considered a first-order approximation to the intermittency in hypersonic flow. Sandborn[32] discussed measurements at Mach 6.7 and 9.4 indicating that the intermittent outer region extended over only about 20% of the boundary-layer thickness. In contrast, the intermittent outer region includes more than 50% of a subsonic boundary layer. This indicates that the intermittency given by Eq. (7), in which γ begins to drop off rapidly about halfway across the boundary layer, is not appropriate in hypersonic flow. According to Bradshaw,[33] "None of the other turbulence properties changes as spectacularly as intermittency" between the low-speed and hypersonic regimes. Recent measurements by Robinson[34] confirm that the fraction of the boundary layer over which intermittency occurs decreases with increasing Mach number. Additional measurements will probably be required before an appropriate intermittency model which accounts for Mach number can be developed.

Beyond the differences due to the forms of the near-wall damping and outer-layer intermittency, the outer eddy viscosities computed by the two models depend largely on the predicted velocity distributions. The CS model employs an integral of streamwise velocity to the edge of the boundary layer to determine the length scale δ^* and velocity scale $(V_T)_e$. The BL model uses (approximately) a derivative of the streamwise velocity profile to form the vorticity function, from which the appropriate length and velocity scales, N_{max} and F_{max}, are obtained. The numerical derivative of the velocity profile computed at discrete grid points is clearly more sensitive than the numerical integration of the profile. This is demonstrated by the ambiguity in defining the peak in $F(N)$.

The present results showed that the Cebeci-Smith model with the compressibility factor in the near-wall damping was quite accurate at Mach 3 and 5. Good predictions were also obtained at Mach 8 when the outer-layer intermittency was adjusted; this requires further study. The empirical "constants" in the Baldwin-Lomax model, however, appear to need re-evaluation at supersonic and hypersonic speeds. Moreover, numerical differentiation of the computed velocity profile is unattractive, particularly near starting and in the vicinity of leeward vortices. Because of their basic similarities, either model should produce good predictions when properly calibrated for supersonic or hypersonic flows. In their present formulations, however, the Cebeci-Smith model appears to have more universality.

Acknowledgments

This work was supported by the Computational Aerodynamics Division, Sandia National Laboratories, Albuquerque, New Mexico. The encouragement of contract monitors Drs. Ken Cole and William Oberkampf is much appreciated. The technical assistance of Dr. Fred Blottner (SNLA) was essential to this work. Starting solutions were provided by Dr. Blottner, Don Larson, Mary Walker, and Pete Kaestner of SNLA. Prof.

John Tannehill and Mr. Dinesh Prabhu of Iowa State University graciously provided the PNS code.

References

[1]Tannehill, J. C., Venkatapathy, E., and Rakich, J. V., "Numerical Solution of Supersonic Viscous Flow Over Blunt Delta Wings," *AIAA Journal,* Vol. 20, Feb. 1982, pp. 203–210.

[2]Helliwell, W. S., Alber, I. E., Dickinson, R. P., and Lubard, S. C., "Turbulent Flow Over Vehicles at Angle of Attack," *AIAA Journal,* Vol. 22, March 1984, pp. 321–322 (also AIAA Paper 82-0027, 1982).

[3]Danberg, J. E., van Gulick, P., and Kim, J., "Turbulence Modeling for Steady Three-Dimensional Supersonic Flows," U.S. Army Ballistic Research Lab., Contract Rept. BRL-CR-553, 1986.

[4]Horstman, C. C., "Prediction of Hypersonic Shock-Wave/Turbulent-Boundary-Layer Interaction Flows," AIAA Paper 87-1367, 1987.

[5]Vuong, S. T. and Coakley, T. J., "Modeling of Turbulence for Hypersonic Flows With and Without Separation," AIAA Paper 87-0286, 1987.

[6]Cebeci, T. and Smith, A. M. O., *Analysis of Turbulent Boundary Layers,* Academic Press, New York, 1974, pp. 92–94, 215–217, 256, 264.

[7]Cebeci, T., Kaups, K., Ramsey, J., and Moser, A., "Calculation of Three-Dimensional Laminar and Turbulent Boundary Layers," *Aerodynamic Analysis Requiring Advanced Computers,* NASA SP-347, 1975, pp. 41–76.

[8]Martellucci, A., Rie, H., and Sontowski, J. F., "Evaluation of Several Eddy Viscosity Models Through Comparison with Measurements in Hypersonic Flows," AIAA Paper 69-0688, 1969.

[9]Widhopf, G. F. and Hall, R., "Transitional and Turbulent Heat-Transfer Measurements on a Yawed Blunt Conical Nosetip," *AIAA Journal,* Vol. 10, Oct. 1972, pp. 1318–1325.

[10]Szema, K. Y. and Lewis, C. H., "Computation of Hypersonic Laminar, Transitional and/or Turbulent Viscous Flow Past Blunt Bodies at Angle of Attack," *Numerical Methods for Non-Linear Problems,* Pineridge Press, Swansea, UK, 1980, pp. 873–884.

[11]Hung, C. M. and MacCormack, R. W., "Numerical Simulation of Supersonic and Hypersonic Turbulent Compression Corner Flows," *AIAA Journal,* Vol. 15, March 1977, pp. 410–416.

[12]Baldwin, B. S. and Lomax, H., "Thin Layer Approximation and Algebraic Model for Separated Turbulent Flows," AIAA Paper 78-0257, 1978.

[13]Rakich, J. V., Vigneron, Y. C., and Agarwal, R., "Computation of Supersonic Viscous Flows Over Ogive-Cylinders at Angle of Attack," AIAA Paper 79-0131, 1979.

[14]Cottrell, C. J. and Chapman, G. T., "An Evaluation of a Parabolized Navier-Stokes (PNS) Code for Cone-Cylinder-Flared Configurations," AIAA Paper 84-2116, 1984.

[15]Weinacht, P., Bernard, J. G., Sturek, W. B., and Hodes, B. A., "PNS Computations for Spinning Shell at Moderate Angles of Attack and for Long L/D Finned Projectiles," AIAA Paper 85-0273, 1985.

[16]Degani, D. and Schiff, L. B., "Computation of Turbulent Supersonic Flows Around Pointed Bodies Having Crossflow Separation," *Journal of Computational Physics,* Vol. 66, Sept.-Oct. 1986, pp. 173–196.

[17]McWherter, M., Noack, R. W., and Oberkampf, W. L., "Evaluation of Boundary Layer and Parabolized Navier-Stokes Solutions for Re-Entry Vehicles," *Journal of Spacecraft and Rockets,* Vol. 23, Jan.-Feb. 1986, pp. 70–78.

[18]Visbal, M. and Knight, D., "The Baldwin-Lomax Turbulence Model for Two-Dimensional Shock-Wave/Boundary-Layer Interactions," *AIAA Journal,* Vol. 22, July 1984, pp. 921–928.

[19]Shang, J. S., "Flow Over a Biconic Configuration with an Afterbody Compression Flap—A Comparative Numerical Study," AIAA Paper 83-1668, 1983.

[20]Sturek, W. B. and Schiff, L. B., "Numerical Simulation of Steady Supersonic Flow Over Spinning Bodies of Revolution," *AIAA Journal,* Vol. 20, Dec. 1982, pp. 1724–1731.

[21]McRae, D. S. and Hussaini, M. Y., "Supersonic Viscous Flow Over Cones at Incidence," *Proceedings of the 6th International Conference on Numerical Methods in Fluid Dynamics,* Tbilisi, USSR, 1978, pp. 385–392.

[22]Ausherman, D. W., Yanta, W. J., and Rutledge, W. H., "Measurements of the Three-Dimensional Boundary Layers on Conical Bodies at Mach 3 and Mach 5," AIAA Paper 83-1675, 1983.

[23]Carver, D. B., "Heat Transfer, Surface Pressure and Flow Field Surveys on Conic and Biconic Models with Boundary Layer Trips at Mach 8—Phases IV and V," Calspan/AEDC Div., Rept. AEDC-TSR-80-V14, 1980.

[24]Kaul, U. K. and Chaussee, D. S., "AWFAL Parabolized Navier-Stokes Code: 1983 AFWAL/NASA Merged Baseline Version," U. S. Air Force Wright Aeronautical Lab., Wright-Patterson AFB, OH, AFWAL-TR-83-3118, 1983.

[25]Barnette, D. and Walker, M. A., Personal communication, 1986.

[26]Blottner, F. G. and Larson, D. E., "Navier-Stokes Code NS3D for Blunt Bodies: A Users Manual," Sandia National Lab., Albuquerque, NM, Rept. SAND 88-0504, 1988.

[27]Keller, H. B., *Numerical Methods for Two-Point Boundary-Value Problems,* Blaisdell, Waltham, MA, 1968, pp. 78–81, 168–171.

[28]Blottner, F. G., "Investigation of Some Finite-Difference Techniques for Solving the Boundary Layer Equations," *Computer Methods in Applied Mechanics and Engineering,* Vol. 6, July 1975, pp. 1–30.

[29]Bushnell, D. M., Cary, A. M., Jr., and Harris, J. E., "Calculation Methods for Compressible Turbulent Boundary Layers—1976," NASA SP-422, 1977.

[30]Shirazi, S. A. and Truman, C. R., "Comparison of Algebraic Turbulence Models for PNS Predictions of Supersonic Flow Past a Sphere-Cone," AIAA Paper 87-0544, 1987.

[31]Goldstein, R. J. (ed.), *Fluid Mechanics Measurements,* Hemisphere, Washington, DC, 1983, pp. 565–569.

[32]Sandborn, V. A., "A Review of Turbulence Measurements in Compressible Flow," NASA TM X-62337, 1974.

[33]Bradshaw, P., "Compressible Turbulent Shear Layers," *Annual Review of Fluid Mechanics,* Vol. 9, 1977, pp. 33–54.

[34]Robinson, S. K., "Space-Time Correlation Measurements in a Compressible Turbulent Boundary Layer," AIAA Paper 86-1130, 1986.